Article

Laser Additive Manufacturing of Bulk Silicon Nitride Ceramic: Modeling versus Integral Transform Technique with Experimental Correlation

Cristian N. Mihailescu [1], Mihai Oane [1], Bogdan A. Sava [1,2], Andrei C. Popescu [1], Mihail Elisa [3], Muhammad Arif Mahmood [4], Natalia Mihailescu [1], Ana V. Filip [1], Sinziana Andreea Anghel [1,5], Ion N. Mihailescu [1] and Carmen Ristoscu [1,*]

1   National Institute for Laser, Plasma and Radiation Physics (INFLPR), 409 Atomistilor Street, 077125 Magurele-Ilfov, Romania
2   Faculty of Applied Chemistry and Materials Science, University Politehnica Bucharest, 313 Splaiul Independentei, 060042 Bucharest, Romania
3   National Institute of Research & Development for Optoelectronics, INOE2000, 409 Atomistilor Street, 077125 Magurele-Ilfov, Romania
4   Mechanical Engineering Program, Texas A&M University at Qatar, Doha P.O. Box 23874, Qatar
5   Faculty of Physics, Bucharest University, 405 Atomistilor Street, 077125 Magurele-Ilfov, Romania
*   Correspondence: carmen.ristoscu@inflpr.ro; Tel.: +40-214-574-491

Abstract: A semi-analytical-numerical solution is theorized to describe the laser additive manufacturing via laser-bulk ceramic interaction modeling. The Fourier heat equation was used to infer the thermal distribution within the ceramic sample. Appropriate boundary conditions, including convection and radiation, were applied to the bulk sample. It was irradiated with a Gaussian spatial continuous mode fiber laser ($\lambda = 1.075$ µm) while a Lambert-Beer law was assumed to describe the laser beam absorption. A close correlation between computational predictions versus experimental results was validated in the case of laser additive manufacturing of silicon nitride bulk ceramics. The thermal field value rises but stays confined within the irradiated zone due to heat propagation with an infinite speed, a characteristic of the Fourier heat equation. An inverse correlation was observed between the laser beam scanning speed and thermal distribution intensity. Whenever the laser scanning speed increases, photons interact with and transfer less energy to the sample, resulting in a lower thermal distribution intensity. This model could prove useful for the description and monitoring of low-intensity laser beam-ceramic processing.

Keywords: laser additive manufacturing; silicon nitride bulk ceramic; integral transform technique; Fourier heat equation; modeling

1. Introduction

Additive manufacturing (AM) has lately received a wide acceptance by numerous industries as it demonstrated unique advantages over conventional manufacturing techniques [1,2]. In the case of metallic materials, via starting from a precursor such as a wire or powder, three-dimensional objects with intricate/unique geometrical characteristics can be 3D printed layer by layer [3–5].This manufacturing procedure opens the opportunities to fabricate a large diversity of objects for a vast variety of world-market applications [1,2]. The shape is first designed into a CAD (Computer Aided Design) software, and the 3D model is transferred into a CAM (Computer Aided Manufacturing) program. Here, the user selects the machine's parameters such as starting/ending points of operation, machine trajectory and speed, processing distance from the surface, processing angle and start/stop instructions of the energy beam. The CAM software generates a processing code based on these instructions that is imported into machine's computer. The machine will then follow

the code and conduct the operation in a single step, thus reducing the fabrication time compared to traditional manufacturing technologies and costs. Moreover, various components could be printed in a single stage, thus eliminating the need for more fabrication steps [6]. Nevertheless, AM operates relatively slow as compared to conventional manufacturing techniques. There exist still multiple defects in the parts fabricated by AM technology, including cracks or low surface quality, resulting in poor mechanical properties [7]. Hence, significant efforts should be carried out to further improve the quality and performance of 3D printed parts.

Different AM techniques have been therefore implemented to print various materials used for technological applications. Recently, selective laser melting (SLM) and sintering (SLS) have been extended to the aerospace and medical fields for the 3D printing of aluminum alloys [7], stainless steel [8], titanium alloys [9,10], cobalt-chrome alloys [11], and nickel alloy [12]. Alumina (Al_2O_3) and zirconia (ZrO_2) ceramics have demonstrated large prospective uses, because of their remarkable mechanical, thermal, and wear resistance properties [13]. Indeed, mechanical properties of ultimate components are highly associated with the thermal distribution during printing. Rapid heating and slow cooling around the laser spot generate a high thermal gradient, thus, leading to phase transformations, difficult to be properly monitored experimentally.

During SLM/SLS printing, ceramics require special care in comparison with metals because of the higher laser absorption coefficient in the Near-IR range [14]. This is doubled by the poorer heat dissipation in ceramics due to lower heat diffusivity/conductivity coefficient values. The higher absorbed heat is therefore confined inside smaller ceramic regions which are overheated and exposed to irreversible damage. These effects are much stronger in mid -IR as e.g. at 10.6 μm CO_2 wavelengths [14]. In particular, Si_3N_4 ceramic possesses a thermal conductivity of 15 W m^{-1} K^{-1} only [13,15], significantly inferior to metals, e.g. 317 W m^{-1} K^{-1} for Au [16]. This substantial difference stays at the origin of a large temperature excursion in the sample, from top to bottom (which can be as large as from 1935 to 234 °C), in the case of Si_3N_4 [16].

Therefore, modeling methods were used for AM parameters' optimization [17]. Two types of modeling approaches are present in the literature, described as either macro- or meso-scale. Hodge et al. [18] selected, via a macro-scale modeling, a complex alternative heat source to predict thermal fields and melt pool dimensions for the SLM printing of 316L stainless steel. The melt pool configuration extended above the unconsolidated powder layer via considering the powder layer's insulating behavior.

King et al. [19] estimated the temperature distribution and residual stresses inside a 6 cm tall prism of 316L stainless steel. They found a congruent trend between simulations and experiment.

Li and Gu [20] reported on the modeling of a titanium alloy powder bed taking into account the parameters variation with temperature, under the action of a special Gaussian distribution laser beam. It was found that the excessive heat was eliminated through the cold sample, resulting in a rapid quenching of the deposited material.

Roberts et al. [21] developed a finite element (FE) thermal model by considering the laser beam absorption coefficient. Element's death and birth techniques were employed for the simulation of the Ti6Al4V alloy depositions.

Marion et al. [22] used the FE method to simulate the direct metal deposition process. It was shown that micro-scale modeling (bead formation) can help to comprehend intricate thermal distribution and melt pool dimensions.

King et al. [18] carried out simulations of laser–powder interaction in the presence of a surface tension. It was shown that the surface tension plays an important role in smoothening the melt pool which results in an improved heat transfer coefficient.

One of the major limits of the FE models is that the solutions are primarily dependent on the mesh quality and accuracy, which directly controls the computation efficiency and time. A finer mesh requires a longer computing time as compared to a coarse mesh.

In the present study, an integral transform technique is applied to the finite domain on laser-ceramic interaction, based on the Fourier heat equation, which involves an infinite thermal wave propagation speed. To the best of our knowledge, there are no other reported studies in laser-ceramic interaction using the integral transform technique for the Fourier heat equation. A simplified model was developed with forced convection: $h = 2.4 \times 10^{-3} E T_m^{1.61}$ [15], where E is the material emissivity and T_m is the melting temperature.

We consider the main progress with this contribution as compared to previous work, a drastic reduction of design/computational time with direct effects on technological costs.

2. Mathematical Model

Figure 1 shows the schematic of laser-ceramic interaction. The laser beam is traveling at a constant speed (v) across a sample with the dimensions length (a) × width (b) × height (c).
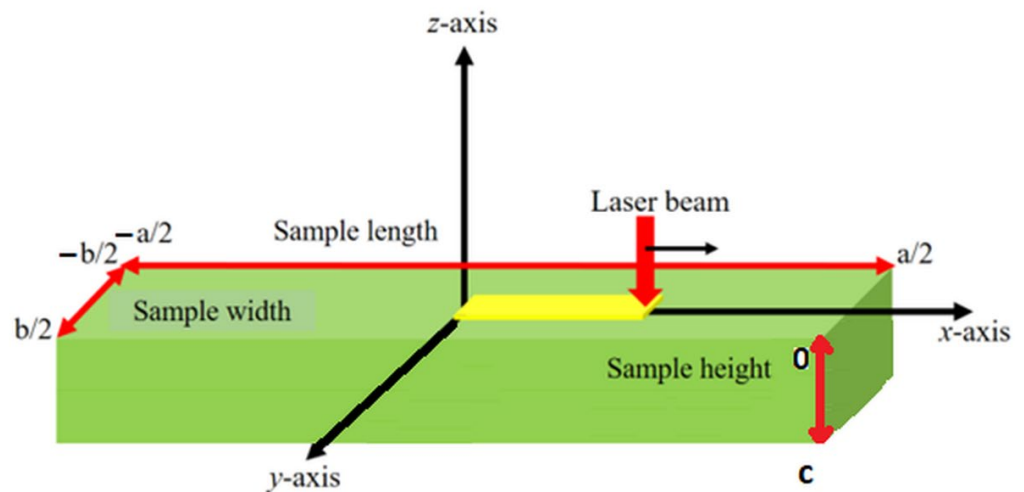

Figure 1. Schematic of the laser beam traveling across a ceramic sample.

The classical Fourier formalism is given in Equation (1), as:

$$\frac{\partial^2 T}{\partial x^2} + \frac{\partial^2 T}{\partial y^2} + \frac{\partial^2 T}{\partial z^2} - \frac{1}{\gamma}\frac{\partial T}{\partial t} = -\frac{A(x,y,z,t)}{k} \tag{1}$$

Here, T stands for the temperature variation inside the sample with Cartesian coordinates (x,y,z), γ is thermal diffusivity, t is time, $A(x,y,z,t)$ is the Gaussian heat source while k is the thermal conductivity of the sample. The boundary and limit conditions are defined by Equations (2)–(4):

$$\left[\frac{\partial T}{\partial x} + \frac{h}{k}T\right]_{x=\frac{-a}{2}} = 0; \quad \left[\frac{\partial T}{\partial x} + \frac{h}{k}T\right]_{x=\frac{a}{2}} = 0 \tag{2}$$

$$\left[\frac{\partial T}{\partial y} + \frac{h}{k}T\right]_{y=\frac{-b}{2}} = 0; \quad \left[\frac{\partial T}{\partial y} + \frac{h}{k}T\right]_{y=\frac{b}{2}} = 0 \tag{3}$$

$$\left[\frac{\partial T}{\partial z} - \frac{h}{k}T\right]_{z=0} = 0; \quad \left[\frac{\partial T}{\partial x} + \frac{h}{k}T\right]_{z=c} = 0 \tag{4}$$

Based on the standard theory [23,24], Equations (2)–(4) imply Equations (5)–(7), calculated as:

$$\left[\frac{\partial K_x}{\partial x} + \frac{h}{k}K_x\right]_{x=\frac{-a}{2}} = 0; \quad \left[\frac{\partial K_x}{\partial x} + \frac{h}{k}K_x\right]_{x=\frac{a}{2}} = 0 \tag{5}$$

$$\left[\frac{\partial K_y}{\partial y} + \frac{h}{k}K_y\right]_{y=\frac{-b}{2}} = 0; \quad \left[\frac{\partial K_y}{\partial y} + \frac{h}{k}K_y\right]_{y=\frac{b}{2}} = 0 \tag{6}$$

$$\left[\frac{\partial K_z}{\partial z} - \frac{h}{k}K_z\right]_{z=0} = 0; \quad \left[\frac{\partial K_z}{\partial z} + \frac{h}{k}K_z\right]_{z=c} = 0 \tag{7}$$

The term source is defined by Equation (8), as:

$$A(x,y,z,t) = \frac{P}{\pi r_o^2} e^{\frac{-((vt_o+x)^2+y^2)}{r_o^2}} \left(e^{-\alpha z}(1-r_s) + r_s\delta(z)\right)(H(t) - H(t-t_o)); \ t_o = \frac{x}{v} \tag{8}$$

Here, P is the incident laser power, r_o is the laser beam waist radius, α is the laser absorption coefficient, r_s is the sample's surface absorption coefficient, δ is the Dirac-delta function, H is the Heaviside step function, t_o is the material exposure time to laser irradiation, and v is the propagation speed of the laser beam. The correction term can prove useful in quite intricate interactions between the laser beam and solid sample.

The Eigenfunctions K_x, K_y, and K_z along, x-, y- and z-axes, respectively, are expressed as:

$$K_x(\alpha_i, x) = cos(\alpha_i x) + \frac{h}{k\alpha_i}sin(\alpha_i x) \tag{9}$$

$$K_y(\beta_j, y) = cos(\beta_j y) + \frac{h}{k\beta_j}sin(\beta_j y), \tag{10}$$

$$K_z(\chi_o, z) = cos(\chi_o z) + \frac{h}{k\chi_o}sin(\chi_o, z) \tag{11}$$

In Equations (9)–(11), α_i, β_j and χ_o stand for the Eigenvalues, which are calculated numerically by substituting Equations (9)–(11) into Equations (5)–(7), resulting in Equations (12)–(14):

$$2cot\left(\frac{\alpha_i a}{2}\right) = \frac{h}{k\alpha_i} - \frac{\alpha_i k}{h} \tag{12}$$

$$2cot\left(\frac{\beta_j b}{2}\right) = \frac{h}{k\beta_j} - \frac{\beta_j k}{h} \tag{13}$$

$$2cot(\chi_o c) = \frac{\chi_o k}{h} - \frac{h}{k\chi_o} \tag{14}$$

The thermal variation inside ceramic samples, under laser irradiation, is calculated as:

$$\begin{aligned}
T(&x,y,z,t) \\
&= \sum_{i=1}^{\infty}\sum_{j=1}^{\infty}\sum_{o=1}^{\infty}\left[\frac{1}{C_iC_jC_o}\int_{\frac{-a}{2}}^{\frac{a}{2}}\int_{\frac{-b}{2}}^{\frac{b}{2}}\int_0^c \frac{P}{\pi r_o^2}e^{\frac{-(x^2+y^2)}{r_o^2}}\frac{1}{\alpha_i^2+\beta_j^2+\chi_o^2}\left[1-e^{-\gamma_{ijo}^2 t}\right.\right. \\
&\left.-\left(1-e^{-\gamma_{ijo}^2\left(t-\frac{x}{v}\right)}\right)\right]H\left(t-\frac{x}{v}\right)\left[e^{-\alpha z}(1-r_s)\right. \\
&\left.\left.+r_s\delta(z)\right]K(\alpha_i,x)K(\beta_j,y)K(\chi_o,z)\right]dxdydzK(\alpha_i,x)K(\beta_j,y)K(\chi_o,z),
\end{aligned} \tag{15}$$

where

$$\gamma_{ijo}^2 = \gamma\left(\alpha_i^2 + \beta_j^2 + \chi_o^2\right) \tag{16}$$

and

$$C_i = \int_{\frac{-a}{2}}^{\frac{a}{2}} K^2(\alpha_i, x)dx; \ C_j = \int_{\frac{-b}{2}}^{\frac{b}{2}} K^2(\beta_j, y)dy; \ C_o = \int_0^c K^2(\chi_o, z)dz \tag{17}$$

One notes that Equations (15)–(17) are in fact a combination of analytical and numerical solutions. However, for simulations, only the first three Eigen values (i = 1,2,3, j = 1,2,3 and k = 1,2,3) have been considered, which yield a semi-analytical-numerical solution.

3. Methodology and Simulations

Silicon nitride (Si_3N_4) bulk samples were chosen for simulations, but the method can be easily extended to other ceramics compounds. One should mention here that Si_3N_4

was under extensive research in recent decades, in particular under the action of laser Gaussian beams.

Thus, Shukla and Lawrence [15,16] carried out processing experiments with a continuous wave fiber laser (λ = 1.075 μm) and FE simulations in the case of Si_3N_4 samples with 50 mm length, 10 mm width, and 10 mm height. Other authors reported on laser additive manufacturing (LAM) of Si_3N_4 using CO_2 laser (λ = 10.6 μm) [25] or yttria laser radiation (λ= 1.07 μm) [26], respectively. Table 1 collects the Si_3N_4 characteristics but also the parameters used in computations.

Table 1. Silicon nitride bulk characteristics and simulation conditions [15].

Parameter Name	Value (Units)
Density	3200 (kg/m^3)
Room temperature	25 (°C)
Specific heat	900 (J/kg-K)
Thermal conductivity	15 (W/mK)
Laser absorption coefficient	0.90
Laser beam spot diameter	3.0 (mm)
Emissivity	0.40
Laser wavelength	1.075 (μm)
Type of laser	Continuous wave Fiber laser

A Core i7, 8th Generation processor equipped with a 32 GB Ram computation system has been used for analytical simulations. A user-defined script file was written in MATHEMATICA software (9.0, Wolfram, Champaign, IL, USA).

4. Results and Discussion

Initially, the laser beam was positioned in the center of the sample while the *x*-, *y*-, and *z*-axes define its length, width, and height. Figure 2a presents the 3D thermal field distribution plot when laser power and laser scanning speed are 143.25 W and 0 mm/min, respectively. When the laser beam started to irradiate, the sample's temperature instantly increased up to 2000 °C due to the infinite speed of the heat wave, as visible also from Figure 2b. This behavior occurred because the Fourier heat equation can take into account all corrections related to laser-sample interaction. Furthermore, one can identify the perfect symmetrical shape of the thermal profile that is due to the Gaussian heat source at a laser scanning speed of 0 mm/min.

(**a**)

(**b**)
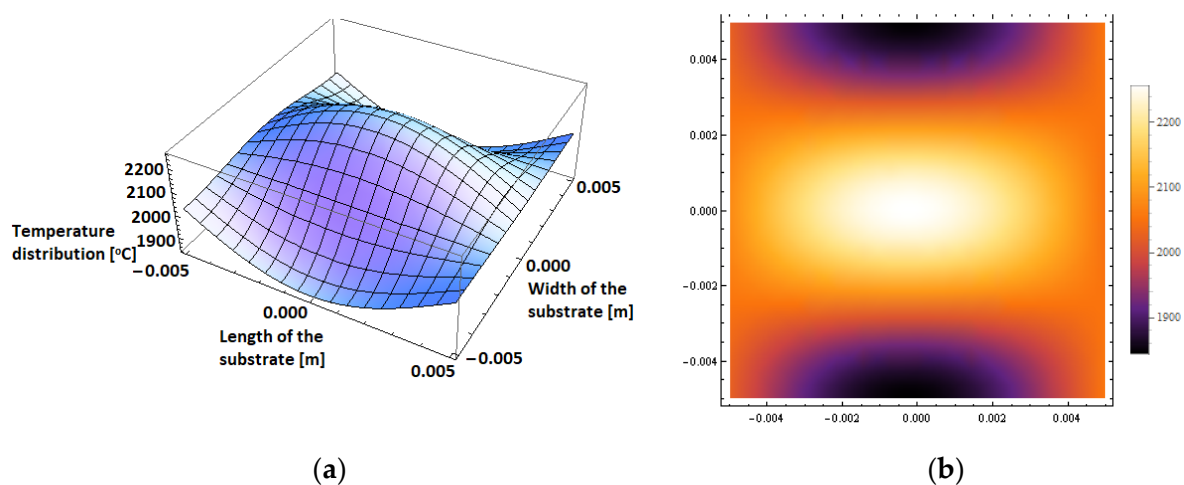
Figure 2. Symmetrical 3D thermal field for laser-Si_3N_4 interaction in the case of 143.25W laser power and 0 mm/min laser scanning speed (**a**) and 2D plot of the temperature distribution (**b**).

Figure 3 shows the thermal distribution in the melt pool when laser power = 143.25 W and laser scanning speed = 100 mm/min, respectively. One can observe that the thermal distribution reaches the maximum at the top of the sample where the laser beam is in direct contact with the material. As the sample thickness is small (of 10 mm only), the thermal distribution remains almost constant into the melt pool depth.
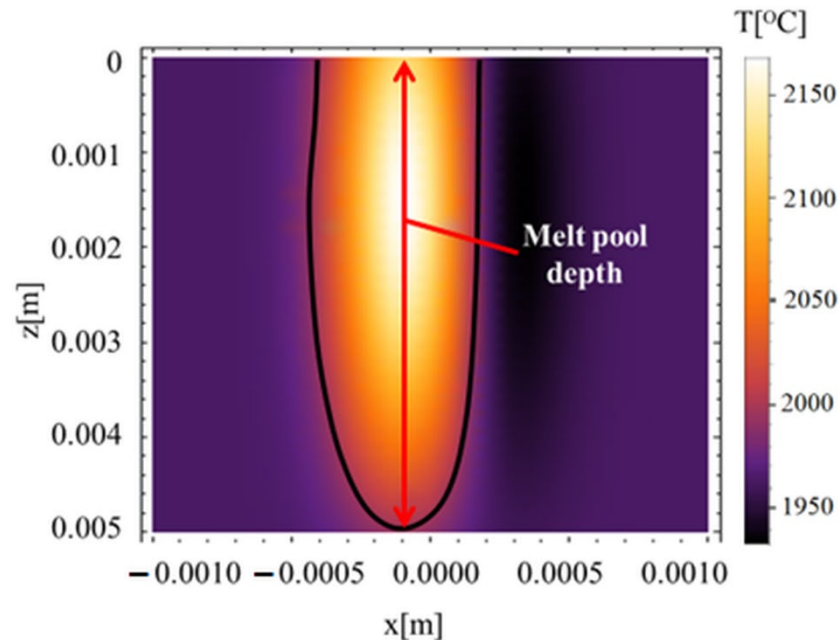
Figure 3. Symmetrical 2D thermal field across the ceramic sample for laser-Si3N4 interaction when laser power = 143.25 W and laser scanning speed = 100 mm/min.

To validate the laser-bulk ceramic interaction model, Table 2 presents a comparison between current simulation, FE simulation, and experimental results in the case of laser-Si_3N_4 sample interaction for a laser power of 143.25 W and a laser scanning speed of 100 mm/min. The FE simulation and experimental results are from the paper by Shukla and Lawrence [15]. One can notice in Table 2 that our model can predict outcomes with an accuracy of 1.05% mean absolute deviation.

Table 2. Maximum temperature in the case of current simulation, FE simulation and experimental results [15] for laser—Si_3N_4 sample interaction.

Laser Power (W)	Laser Scanning Speed (mm/min)	Maximum Temperature in the Case of Current Simulation (°C)	Maximum Temperature in the Case of FE Simulation [15] (°C)	Maximum Temperature in Experiments [15] (°C)
143.25	100	2245	2236	2269

It was found that 143.25 W at 100 mm/min was the best in terms of achieving a surface with minimal defects [15] and was therefore selected for further processing.

Figure 4 displays the thermal field 3D and 2D plots when the laser scanning speed increases from 150 (Figure 4a,b) to 200 mm/min (Figure 4c,d), respectively, for the same laser power of 143.25 W. One notices that with the increment in laser scanning speed, the thermal distribution intensity decreases drastically. This is because, when the laser scanning speed increases, a lower number of photons interact with the ceramic sample and transfer less energy to a given side, which results in the thermal distribution intensity reduction. One may observe that our model fails for lower temperature at a laser speed of 200 mm/min.

(a)

(b)

(c)

(d)
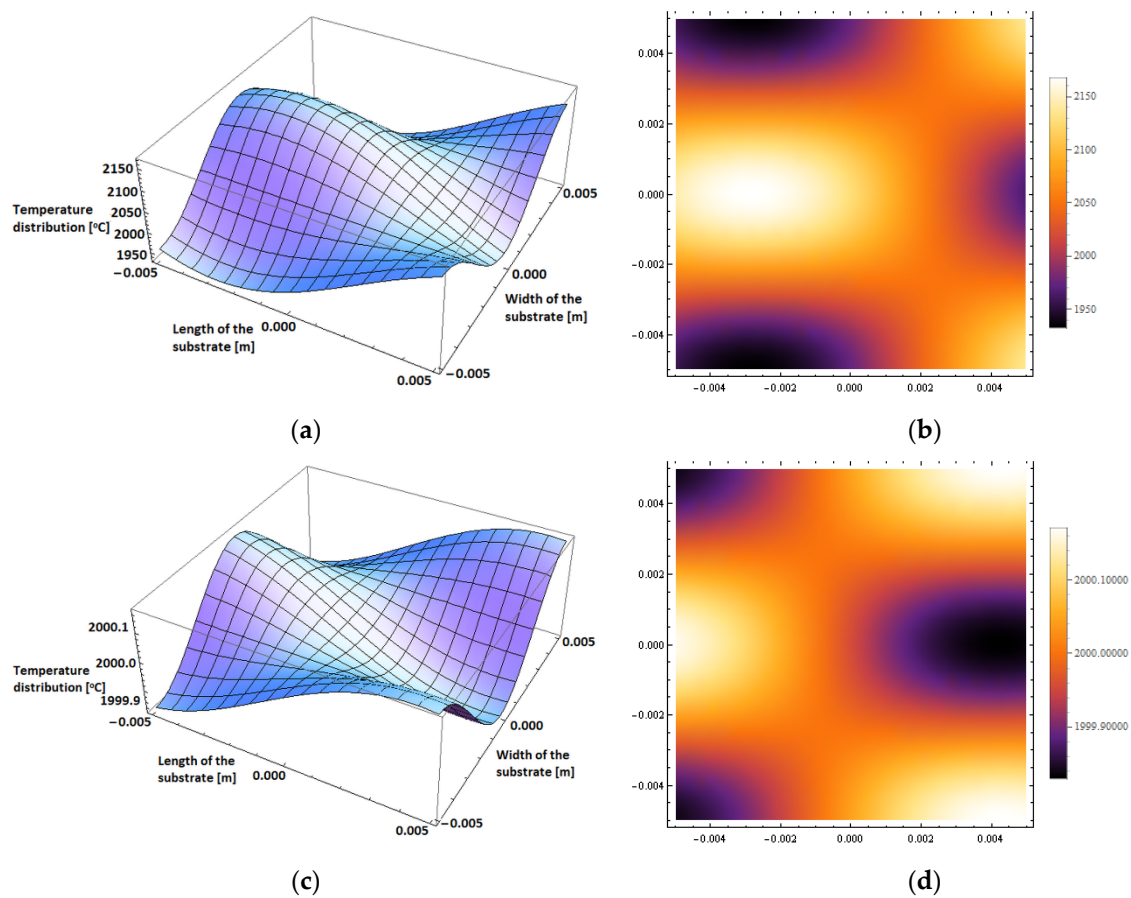
Figure 4. Thermal field in the case of laser- Si_3N_4 interaction for a laser power of 143.25 W and a laser scanning speed of 150 mm/min (**a**,**b**) and 200 mm/min (**c**,**d**), respectively.

An agreement between our simulation and experimental results in [15] shows a deviation of 1.05% only, which is quite close to 1.45% accuracy between the simulations and experiments in that reference. One should note here that P.P. Shukla and J. Lawrence simulations are pure numerical in comparison with ours which are semi-analytical-numerical. It is, therefore, worth mentioning that the simulation time when using our model was of 10 min only, significantly inferior to Shukla and Lawrence's simulation of about 2 h [15].

Moreover, our model can be considered a very powerful one but also a very friendly to use: for writing the software one may need 20 min and on the other hand the run time of a complete simulation is down than 10 min on a commercial PC (which is much lower than the usual time for numerical models [15,27–30]).

Finally, one should notice that the applied model is similar in the case of metals and ceramics but the heat transfer coefficients make the difference. It mathematically follows that the Eigen functions in the case of ceramics are superior to those of metals. This is due to both higher absorption of laser energy and lower dissipation of heat as also mentioned in Ref. [14]. This is proved by numerous computer simulations and mathematical considerations.

5. Conclusions

A semi-analytical-numerical model has beenwas developed to describe the interaction of a Gaussian laser beam with a bulk ceramic sample. The Fourier heat equation was applied to determine the thermal distribution within the laser irradiated sample. The convection and radiation boundary conditions were taken into account. The simulation results are also in good accordance with that reported in.

The main conclusions can be summarized as follows.

- The thermal field value increases rapidly at the irradiation site due to the heat propagation with an infinite speed (Fourier equation). The thermal conductivity in ceramics stays lower compared to metals, thereby limiting the heat expansion within the surrounding zones resulting in heat accumulation and a very high temperature rise.
- A correlation was shown between the laser scanning speed and thermal distribution intensity. Thus, whenever the laser scanning speed increases, less photons interact and transfer energy to the sample, resulting in a lower thermal distribution intensity.
- In laser additive manufacturing of ceramics, the laser beam energy absorption is split via surface or during propagation trough bulk, respectively. This depends on surface morphology, crystalline status, and processing history.

One may use the results of this study to optimize the operating conditions when designing accurate and efficient laser additive manufacturing processing of bulk ceramics.

Author Contributions: Conceptualization, A.C.P., M.O., N.M. and M.A.M.; methodology, M.O., C.N.M. and M.A.M.; software, M.O., A.V.F. and M.A.M.; validation, M.O., M.A.M., N.M., I.N.M. and C.R.; formal analysis, M.O., B.A.S., M.E., M.A.M., C.N.M., S.A.A. and C.R.; investigation, M.O., M.A.M., A.V.F., S.A.A. and C.R.; resources, A.C.P., C.R., C.N.M. and I.N.M.; data collection, M.O., C.N.M., N.M. and M.A.M.; writing-original draft preparation, M.O., B.A.S., M.E., M.A.M., I.N.M. and C.R.; writing-review and editing, M.O., M.A.M., N.M., C.N.M., A.V.F., A.C.P., I.N.M. and C.R.; supervision, A.C.P., C.R. and I.N.M.; project administration, A.C.P., C.R., C.N.M. and I.N.M.; funding acquisition, C.R., C.N.M. and I.N.M. All authors have read and agreed to the published version of the manuscript.

Institutional Review Board Statement: Not applicable.

Informed Consent Statement: Not applicable.

Data Availability Statement: Not applicable.

Conflicts of Interest: The authors declare no conflict of interest.

References

1. Mahmood, M.A.; Popescu, A.C.; Mihailescu, I.N. Metal Matrix Composites Synthesized by Laser-Melting Deposition: A Review. *Materials* **2020**, *13*, 2593. [CrossRef] [PubMed]
2. Mahmood, M.A.; Popescu, A.C.; Oane, M.; Ristoscu, C.; Chioibasu, D.; Mihai, S.; Mihailescu, I.N. Three-Jet Powder Flow and Laser–Powder Interaction in Laser Melting Deposition: Modelling Versus Experimental Correlations. *Metals* **2020**, *10*, 1113. [CrossRef]
3. Sing, S.L. Perspectives on Additive Manufacturing Enabled BetaTitanium Alloys for Biomedical Applications. *Int. J. Bioprint.* **2022**, *8*, 478. [CrossRef]
4. Amit Bandyopadhyay, Yanning Zhang & Bonny Onuike, Additive Manufacturing of Bimetallic Structures. Available online: https://www.tandfonline.com/loi/nvpp20 (accessed on 15 June 2022).
5. Gong, X.; Zeng, D.; Groeneveld-Meijer, W.; Manogharan, G. Additive manufacturing: A machine learning model of process-structure-property linkages for machining behavior of Ti-6Al-4V, Additive manufacturing: A machine learning model of process-structureproperty linkages for machining behavior of Ti-6Al-4V. *Mater. Sci. Add. Manuf.* **2022**, *1*, 6. [CrossRef]

6.   Mahmood, M.A.; Popescu, A.C.; Hapenciuc, C.L.; Ristoscu, C.; Visan, A.I.; Oane, M.; Mihailescu, I.N. Estimation of clad geometry and corresponding residual stress distribution in laser melting deposition: Analytical modeling and experimental correlations. *Int. J. Adv. Manuf. Technol.* **2020**, *111*, 77–91. [CrossRef]

7.   Olakanmi, E.O.; Cochrane, R.F.; Dalgarno, K.W. A review on selective laser sintering/melting (SLS/SLM) of aluminium alloy powders: Processing, microstructure, and properties. *Prog. Mater. Sci.* **2015**, *74*, 401–477. [CrossRef]

8.   Akita, M.; Uematsu, Y.; Kakiuchi, T.; Nakajima, M.; Kawaguchi, R. Defect-dominated fatigue behavior in type 630 stainless steel fabricated by selective laser melting. *Mater. Sci. Eng. A* **2016**, *666*, 19–26. [CrossRef]

9.   Schwab, H.; Palm, F.; Kühn, U.; Eckert, J. Microstructure and mechanical properties of the near-beta titanium alloy Ti-5553 processed by selective laser melting. *Mater. Des.* **2016**, *105*, 75–80. [CrossRef]

10.   Liu, Y.J.; Li, S.J.; Wang, H.L.; Hou, W.T.; Hao, Y.L.; Yang, R.; Sercombe, T.B.; Zhang, L.C. Microstructure, defects and mechanical behavior of beta-type titanium porous structures manufactured by electron beam melting and selective laser melting. *Acta Mater.* **2016**, *113*, 56–67. [CrossRef]

11.   Averyanova, M.; Bertrand, P.; Verquin, B. Manufacture of Co-Cr dental crowns and bridges by selective laser Melting technology. *Virtual Phys. Prototyp.* **2011**, *6*, 179–185. [CrossRef]

12.   Harrison, N.J.; Todd, I.; Mumtaz, K. Reduction of micro-cracking in nickel superalloys processed by Selective Laser Melting: A fundamental alloy design approach. *Acta Mater.* **2015**, *94*, 59–68. [CrossRef]

13.   Konrad, W. Net Shaped High Performance Oxide Ceramic Parts by Selective Laser Melting. *Phys. Procedia* **2010**, *5*, 587–594. [CrossRef]

14.   Li, J.F.; Li, L.; Stott, F.H. Comparison of volumetric and surface heating sources in the modeling of laser melting of ceramic materials. *Int. J. Heat Mass Transf.* **2004**, *47*, 1159–1174. [CrossRef]

15.   Shukla, P.P.; Lawrence, J. Examination of temperature distribution and the thermal effects on Si3N4 engineering ceramics during fibre laser surface treatment. *Opt. Lasers Eng.* **2011**, *49*, 998–1011. [CrossRef]

16.   Shukla, P.P.; Lawrence, J. Investigation of Temperature Distribution During CO2 Laser and Fibre Laser Processing of a Si_3N_4 Engineering Ceramic by Means of a Computational and Experimental Approach. *Lasers Eng.* **2013**, *27*, 135–160.

17.   Bucă, A.M.; Oane, M.; Mahmood, M.A.; Mihăilescu, I.N.; Popescu, A.C.; Sava, B.A.; Ristoscu, C. Non-fourier estimate of electron temperature in case of femtosecond laser pulses interaction with metals. *Metals* **2020**, *10*, 606. [CrossRef]

18.   Hodge, N.E.; Ferencz, R.M.; Solberg, J.M. Implementation of a thermomechanical model for the simulation of selective laser melting. *Comput. Mech.* **2014**, *54*, 33–51. [CrossRef]

19.   King, W.; Anderson, A.T.; Ferencz, R.M.; Hodge, N.E.; Kamath, C.; Khairallah, S.A. Overview of modelling and simulation of metal powder bed fusion process at Lawrence Livermore National Laboratory. *Mater. Sci. Technol.* **2015**, *31*, 957–968. [CrossRef]

20.   Li, Y.; Gu, D. Thermal behavior during selective laser melting of commercially pure titanium powder: Numerical simulation and experimental study. *Addit. Manuf.* **2014**, *1*, 99–109. [CrossRef]

21.   Roberts, I.A.; Wang, C.J.; Esterlein, R.; Stanford, M.; Mynors, D.J. A three-dimensional finite element analysis of the temperature field during laser melting of metal powders in additive layer manufacturing. *Int. J. Mach. Tools Manuf.* **2009**, *49*, 916–923. [CrossRef]

22.   Marion, G.; Cailletaud, G.; Colin, C.; Mazière, M. A finite element model for the simulation of direct metal deposition. In Proceedings of the International Congress on Applications of Lasers & Electro-Optics, Laser Institute of America, Orlando, FL, USA, 14–18 October 2018; pp. 834–841. [CrossRef]

23.   Oane, M.; Mahmood, M.A.; Popescu, A. A State-of-the-Art Review on Integral Transform Technique in Laser-Material Interaction: Fourier and Non-Fourier Heat Equations. *Materials* **2021**, *14*, 4733. [CrossRef] [PubMed]

24.   Mihăilescu, C.N.; Oane, M.; Mihăilescu, N.; Ristoscu, C.; Mahmood, M.A.; Mihăilescu, I.N. A New Approach to Solve Non-Fourier Heat Equation via Empirical Methods Combined with the Integral Transform Technique in Finite Domains. In *Matrix Theory—Classics and Advances*; IntechOpen: Rijeka, Croatia, 2022. [CrossRef]

25.   Wei, Z.-H.; Cheng, L.-J.; Ma, Y.-X.; Chen, A.-N.; Guo, X.-F.; Wu, J.-M.; Shi, Y.-S. Direct fabrication mechanism of pre-sintered Si_3N_4 ceramic with ultra-high porosity by laser additive manufacturing. *Scr. Mater.* **2019**, *173*, 91–95. [CrossRef]

26.   Minasyan, T.; Liu, L.; Aghayana, M.; Kollo, L.; Kamboj, N.; Aydinyan, S.; Hussainova, I. A novel approach to fabricate Si_3N_4 by selective laser melting. *Ceram. Int.* **2018**, *44*, 13689–13694. [CrossRef]

27.   Chen, H.; Sun, Y.; Yuan, W.; Pang, S.; Yan, W.; Shi, Y. A Review on Discrete Element Method Simulation in Laser Powder Bed Fusion Additive Manufacturing. *Chin. J. Mech. Eng. Addit. Manuf. Front.* **2022**, *1*, 100017. [CrossRef]

28.   Bouabbou, A.; Vaudreuil, S. Understanding laser-metal interaction in selective laser melting additive manufacturing through numerical modelling and simulation: A review. *Virtual Phys. Prototyp.* **2022**, *17*, 543–562. [CrossRef]

29.   Zhang, Z.; Modest, M.F. Temperature-Dependent Absorptances of Ceramics for Nd:YAG and CO_2 Laser Processing Applications. *J. Heat Transf.* **1998**, *120*, 322–327. [CrossRef]

30.   Tsarkova, O.G. Optical and Thermal Properties of Metals, Ceramics, and CVD Diamond Films upon High-Temperature Laser Heating. *Phys. Wave Phenom.* **2007**, *15*, 12–45. [CrossRef]